

## Geometry of Reduced Supersymmetric 4D Yang-Mills Integrals

Z. Burda<sup>1,2</sup>, B. Petersson<sup>1</sup> and J. Tabaczek<sup>1</sup>

<sup>1</sup>Fakultät für Physik, Universität Bielefeld  
P.O.Box 100131, D-33501 Bielefeld, Germany

<sup>2</sup>Institute of Physics, Jagellonian University  
ul. Reymonta 4, 30-059 Krakow, Poland

### Abstract

We study numerically the geometric properties of reduced supersymmetric non-compact  $SU(N)$  Yang-Mills integrals in  $D = 4$  dimensions, for  $N = 2, 3, \dots, 8$ . We show that in the range of large eigenvalues of the matrices  $A^\mu$ , the original  $D$ -dimensional rotational symmetry is spontaneously broken and the dominating field configurations become one-dimensional, as anticipated by studies of the underlying surface theory. We also discuss possible implications of our results for the IKKT model.

### Introduction

Reduced supersymmetric Yang-Mills integrals appear in many areas of fundamental physics ranging from  $QCD$  to string theory. An important issue is whether such reduced integrals are able to capture universal properties of the corresponding supersymmetric Yang-Mills theory in the large  $N$  limit, a question similar to the one posed by Eguchi and Kawai in the context of standard  $QCD$  [1, 2]. Reduced supersymmetric Yang Mills integrals also enter calculations of the Witten index [3] of a wide class of supersymmetric quantum mechanical systems in D-brane physics [4, 5]. Finally, in recent years a non-perturbative definition of string theory was proposed in terms of a ten-dimensional reduced supersymmetric Yang-Mills integral – the IKKT model – which is believed to reproduce, in an appropriate large  $N$  limit, amplitudes including all topological contributions of IIB critical strings [6].

As a supersymmetric model, the reduced Yang-Mills integral can be defined in  $D = 3, 4, 6$ , or 10 dimensions. As it turns out, many important

properties of the model, such as the singular behaviour of the field correlators, change with  $D$  in a systematic way, so that results gained for one value of  $D$  can be extrapolated to the other cases. We will in this paper focus on the four-dimensional model. In this case, the effective action, obtained by integrating out the fermionic degrees of freedom, is positive semi-definite which makes it well-suited to Monte Carlo studies.

Analytically, the model – in any dimension – has so far been solved only for  $N = 2$  [3, 5, 7]. For larger  $N$ , there exist some results from approximate analytic methods [8] and numerical simulations [9, 10, 11, 12, 13]. This made it possible to address questions related to the properties of the eigenvalue spectrum [9, 10] as well as the scaling of physical quantities like the gyration radius, correlation functions, and Wilson loops [11, 12, 13].

In this paper, we will study the geometrical properties of the model in more detail. Our motivation comes from earlier studies of the geometrical structure exhibited by the corresponding surface theory [14, 15]. This model was examined numerically in a discretized form, using the dynamical triangulation approach [16, 17]. The distribution of the gyration radius was found to have a power-like tail.

For the matrix model one expects the same kind of large  $R$  behaviour. More precisely, the analytic solution for  $N = 2$  exhibits a tail  $\rho(R) \sim R^{-2D+5}$ , and it was conjectured from results of the one-loop approximation that this formula should also hold for any  $N > 2$ . Intriguingly, in the surface theory for  $D = 4$  one observes  $\rho(R) \sim R^{-3}$ , which agrees with the result from the matrix model. A mechanism was proposed to explain the appearance of this tail, relying on the emergence of essentially one-dimensional configurations called ‘needles’ or ‘tubes’. Numerical simulations for  $D = 4$  were able to show that such configurations do indeed dominate the large  $R$  part of the  $\rho(R)$  distribution. If one assumes the dominance of the ‘tubes’ for any  $D$ , one finds exactly the same formula as in the matrix model,  $\rho(R) \sim R^{-2D+5}$ .

An obvious question that arises at this point is whether the tail that appears in the matrix model could be explained by a similar mechanism, *i. e.* whether the geometrical structure of large eigenvalue configurations also becomes one-dimensional. Trying to answer this question is the central aim of this paper. We will again use numerical simulations to examine this point.

We begin the paper by shortly reviewing the matrix model of reduced Yang-Mills integrals. We then describe the observables that allow us to pick up the geometrical structure of a given configuration, and present the numerical results. We finish with a short discussion.

## The model

The zero-dimensional supersymmetric Yang-Mills integral is defined in the Euclidean sector by the partition function [6]

$$Z = \int dA d\bar{\Psi} d\Psi e^{-S[A, \bar{\Psi}, \Psi]}, \quad (1)$$

where the action is given by

$$S[A, \bar{\Psi}, \Psi] = S_B + S_F = -\frac{1}{4} \text{Tr} [A^\mu, A^\nu]^2 + \frac{1}{2} \text{Tr} \bar{\Psi} \Gamma_\mu [A^\mu, \Psi]. \quad (2)$$

The model is believed to provide a non-perturbative definition of string theory. The  $N \times N$  traceless Hermitean matrices  $A^\mu$ ,  $\mu = 1, \dots, D$ , are a sort of quantum operators for the bosonic coordinates  $X^\mu(\tau, \sigma) \rightarrow A_{ij}^\mu$  of the string world-sheet in the  $D$ -dimensional target space. The fields  $\bar{\Psi}, \Psi$  are fermionic matrices that transform as Majorana-Weyl spinors in  $D = 10$  dimensions, and as Weyl spinors in  $D = 4$ . The IKKT model corresponds to the case  $D = 10$ .

As in any quantum theory, one is interested in measuring correlation functions, the simplest of which are one-matrix correlators of the type  $\langle \frac{1}{N} (\text{Tr} A_\mu^2)^k \rangle$ . Because the model is rotationally invariant, such correlators do not depend on the choice of  $A^\mu$ . More specifically, for any matrix of the form  $A = n_\mu A^\mu$ , where  $n_\mu$  is a unit vector, the correlators give identical results.

One-matrix correlators can be expressed as moments of the distribution of eigenvalues of the  $A^\mu$ ,

$$\left\langle \frac{1}{N} (\text{Tr} A^2)^k \right\rangle = \int d\lambda \rho(\lambda) \lambda^{2k}, \quad (3)$$

where

$$\rho(\lambda) = \left\langle \frac{1}{N} \sum_{n=1}^N \delta(\lambda - \lambda_n) \right\rangle. \quad (4)$$

For  $N = 2$ , the eigenvalue distributions can be found analytically for  $D = 4, 6$  and 10 dimensions [7], and were shown to have the large  $\lambda$  behaviour

$$\rho(\lambda) \sim \lambda^{-2D+5}. \quad (5)$$

For higher  $N$  the integrals have not been solved analytically. However, it was conjectured [7], based on results of the one-loop approximation [8], that

the large  $\lambda$  part of the spectrum should be controlled by the same powers (5) independently of  $N$ .

The power law (5) describes exactly the same behaviour as was found for the surface theory, in which case it was shown that the dominating configurations are one-dimensional [17] with scaleless fluctuations of the extension in the elongated direction.

One way of extracting the dimensionality of the surface model is to measure the correlation matrix

$$C_{\mu\nu} = \frac{\int \sqrt{g} X_\mu X_\nu}{\int \sqrt{g}}. \quad (6)$$

The trace of this matrix gives the square of the gyration radius,

$$R^2 = \sum_\mu C_{\mu\mu} = \frac{\int \sqrt{g} \sum_\mu X_\mu^2}{\int \sqrt{g}}. \quad (7)$$

We can simplify things by choosing a basis in which  $C_{\mu\nu}$  becomes diagonal,

$$C_{ij} = \frac{1}{N} \delta_{ij} r_i^2. \quad (8)$$

In this case,  $R^2 = \sum_i r_i^2$ . Also, the individual eigenvalues  $r_i^2$  now describe the square extent of the system in the directions given by this particular basis.

For large  $R$ , the distribution of  $R$  was found to behave as  $\rho(R) \sim R^{-3}$ , just as in (5). Also, one of the eigenvalues  $r_i^2$  was shown to become much larger than the others, reflecting the one-dimensional nature of the large  $R$  configurations in the surface theory [17].

In analogy to this, we can now try to determine the dimensionality of the matrix model. We can define the quantum correlation matrix as

$$C_{\mu\nu} = \frac{1}{N} \text{Tr} A_\mu A_\nu \quad (9)$$

and the square of the gyration radius  $R^2$  as

$$R^2 = \sum_\mu C_{\mu\mu} = \frac{1}{N} \text{Tr} \sum_\mu A_\mu^2. \quad (10)$$

Given that we can freely rotate the  $A^\mu$  as discussed above, we can again arrange things such that we find a diagonal matrix  $C_{ij}$ , and the gyration radius once more becomes  $R^2 = \sum_i r_i^2$ . The eigenvalues  $r_i^2$  are all real numbers and can again be interpreted as the square extent of the system in the directions  $i$ , except that this time they also include quantum fluctuations.

The effective dimensionality can now be determined from the distribution of the  $r_i^2$ . If  $d$  out of  $D$  eigenvalues can be shown to be much larger than the remaining ones, the system can be said to be effectively  $d$ -dimensional.

Let us order the eigenvalues by size,  $r_i^2 \geq r_{i+1}^2$ . We will study the behaviour of  $r_i^2$  as a function of  $R^2$  :

$$\langle r_i^2 \rangle_{R^2} = \frac{\int e^{-S[A, \bar{\Psi}, \Psi]} \delta(R^2(A) - R^2) r_i^2(A)}{\int e^{-S[A, \bar{\Psi}, \Psi]} \delta(R^2(A) - R^2)} \quad (11)$$

From what we found in the surface model, we expect for large  $R$  to see  $\langle r_1^2 \rangle_{R^2} \sim R^2$  whereas the other  $\langle r_i^2 \rangle_{R^2}$  should, in comparison, become negligible. It is convenient to introduce a new observable

$$\eta = \frac{r_2^2 + r_3^2 + r_4^2}{R^2} = 1 - \frac{r_1^2}{R^2} \quad (12)$$

as a quantitative measure of this asymmetry. It tells us which fraction of the square extent of the system comes from the transverse directions. If the system does indeed become one-dimensional for large  $R$ , we should find  $\langle \eta \rangle_{R^2} \rightarrow 0$  for  $R^2 \rightarrow \infty$ .

## Computational method

Using the chiral representation of the gamma matrices and replacing the bispinors  $\Psi$  by two-component spinors  $\psi$

$$\bar{\Psi} = (0, \bar{\psi}) , \quad \Psi = \begin{pmatrix} \psi \\ 0 \end{pmatrix} \quad (13)$$

we can re-write the fermionic part of the action as

$$S_F = \frac{1}{2} \bar{\psi}_{ij}^a \mathcal{M}_{aij,bkn} \psi_{kn}^b \quad (14)$$

where the matrix  $\mathcal{M}$  is given by

$$\mathcal{M}_{aij,bkn} = A_{jk}^\mu \gamma_\mu^{ab} \delta_{ni} - A_{ni}^\mu \gamma_\mu^{ab} \delta_{kj} \quad (15)$$

and the gamma matrices are  $\gamma_\mu = (-i\sigma_0, \vec{\sigma})$ . Here, space-time indices are denoted by Greek letters, matrix indices by  $i, j, k, \dots$ , and spinor indices by  $a, b, c, \dots$ . Each combination of sub-indices  $a, i, j$  forms a single index  $A = \{aij\}$  of the matrix  $\mathcal{M}_{AB}$ . Since the possible values for the sub-indices are  $a = 1, 2$  and  $i, j = 1, \dots, N$ ,  $\mathcal{M}$  is, for now, a  $2N^2 \times 2N^2$  matrix.

However, as it stands  $\mathcal{M}$  has a pair of zero eigenvalues coming from a zero mode of the fermionic action, which is invariant under a change  $\psi \rightarrow \psi + \epsilon \mathbb{1}$ . This zero mode can be removed by omitting, in the partition function, the integration over one of the diagonal elements of the  $\psi$  matrices, for example  $\psi_{NN}$ . This amounts to calculating the fermionic integral for a sub-matrix of  $\mathcal{M}$  in which the two rows and columns corresponding to  $i = j = N$  have been crossed out. Call the determinant of this sub-matrix  $\det_{\mathbb{F}}(\mathbf{A})$ . It is easily checked that  $\det_{\mathbb{F}}(\mathbf{A})$  is always real and positive semi-definite.

After integration over the fermions, the partition function becomes

$$Z = \int \mathcal{D}A e^{-S_B(A)} \det_{\mathbb{F}}(\mathbf{A}) \quad (16)$$

where the integration measure is given by

$$\mathcal{D}A = \prod_{\mu} \left( \prod_{i>j} d\text{Re}(A_{ij}^{\mu}) d\text{Im}(A_{ij}^{\mu}) \right) \left( \prod_i dA_{ii}^{\mu} \right) \delta(\text{Tr}A^{\mu}) \quad (17)$$

The most practical way to deal with the global constraints  $\text{Tr}A^{\mu} = 0$  in (17) is to just ignore them in the simulations, taking  $A^{\mu}$  to be arbitrary Hermitean matrices. This creates a new zero mode in the bosonic sector, since the action is now invariant under the change  $A^{\mu} \rightarrow A^{\mu} + a^{\mu} \mathbb{1}$ , which manifests as a random walk of  $\text{Tr}A^{\mu}$  in the simulations. However, this can easily be corrected by simply subtracting the trace from the matrices before each measuring step,

$$A_{ii}^{\mu} \rightarrow A_{ii}^{\mu} - \frac{1}{N} \text{Tr}A^{\mu}. \quad (18)$$

Physically, this means that we always take measurements in a reference frame that is fixed to the system's center of mass. In the surface theory, the shift corresponds to replacing  $X^{\mu} \rightarrow X^{\mu} - X_{CM}^{\mu}$ .

To update the fields we use a standard Metropolis algorithm. Each updating step consists of randomly choosing one element of each matrix  $A^{\mu}$  and proposing a change by a random number taken from a uniform distribution in a range  $[-\epsilon, \epsilon]$ , where  $\epsilon$  is adjusted so as to produce reasonable acceptance rates. We accept or reject the change according to the Metropolis criterion.

## Results

A first, easy test of our program consists of measuring the average bosonic action, which we know from general scaling arguments should behave as  $\langle S_B \rangle = 3/2(N^2 - 1)$ .

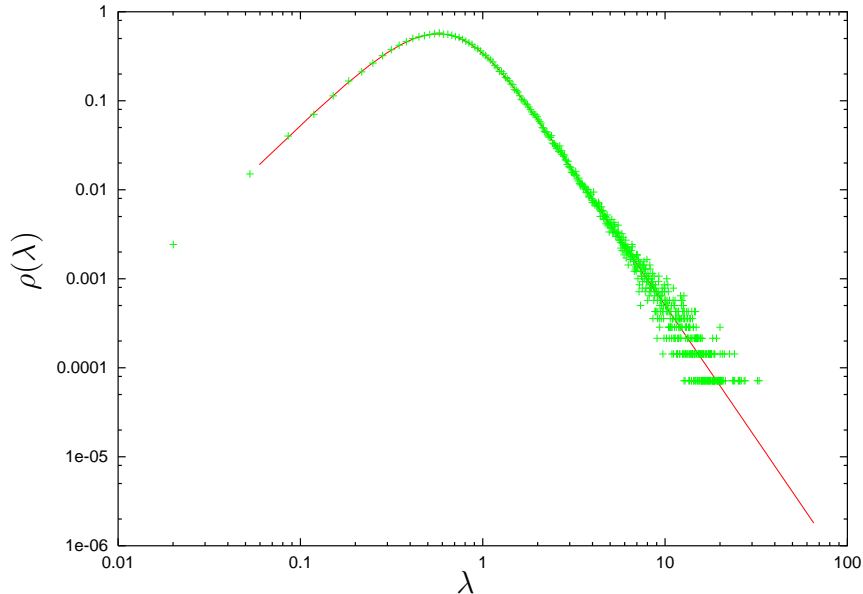


Figure 1: The distribution of eigenvalues from the theoretical prediction (solid line) and the numerical data (crosses). The scale is logarithmic on both axes.

Secondly, we compared the distribution of eigenvalues of  $A^\mu$  to the theoretical formula for  $N = 2$  [7],

$$\rho(\lambda) = 3\sqrt{\frac{2}{\pi}}\lambda^2 U\left(\frac{5}{4}, \frac{1}{2}, 4\lambda^4\right), \quad (19)$$

where  $U$  is the Kummer U-function. The numerical results are shown, together with the theoretical curve, in figure 1.

For large  $\lambda$  (large  $R^2$ ) the quality of the numerical data is limited by two factors. For one thing, the number of data points in this range is very small as the tail, although long, contains only a small fraction of the whole distribution ( $\approx 2.64\%$  for  $|\lambda| > 4$ ). Thus, it takes a long time for the algorithm to produce reasonable statistics in this region. Secondly, the power of the tail is, in absolute values, not very large, which means that once the algorithm does enter the tail, it embarks on a random walk with long excursions that increase the autocorrelation time enormously. Despite these limitations, however, the figure shows quite good agreement between the theoretical curve and the simulation data even within the tail.

Generally, it is known that for the reasons just given it is extremely difficult to deal with power-like fall-offs in numerical simulations. To improve

the quality of the data in this region, we can set a lower limit  $R_{min}^2$  on  $R^2$  to prevent the algorithm from going to the bulk of the distribution, where it would spend almost all of its time otherwise. The price to pay for such a cut-off is a decrease in the acceptance rate of the algorithm as it frequently tries to push through this boundary and go back to the main part. In practice, however, the drop in the acceptance rate turns out to be not too severe. For example, with  $N = 4$  and  $\epsilon = 0.1$  the acceptance rate decreases from 74% to 24% after imposing a lower barrier of  $R_{min}^2 = 120$ .

Similarly, to prevent the algorithm from making too long excursions into the comparatively flat tail of the distribution we can introduce an upper limit  $R_{max}^2$ . As expected, this drastically reduces the autocorrelation time.

We measured the asymmetry parameter  $\eta$  and the distribution of the squared gyration radius  $R^2$  for  $N = 2, \dots, 8$ . For each value of  $N$  we performed  $10^5$  measurements (or  $4 \times 10^4$  in the case of  $N = 8$ ), each separated by 100 sweeps, where a sweep encompasses  $N^2$  Metropolis trials. As an example, for  $N = 4$ , we found an integrated autocorrelation time for  $R^2$ , calculated in units of 100 sweeps, of  $\tau_{R^2} = 130(10)$ .

Let us start with a discussion of the results from the  $N = 2$  case. From the analytic solution ([3, 5]), we find for the distribution of the eigenvalues of  $C_{\mu\nu}$  :

$$\rho(r) \sim (r_1 r_2 r_3)^\alpha (r_1^2 - r_2^2)(r_2^2 - r_3^2)(r_3^2 - r_1^2) e^{-2(r_1^2 r_2^2 + r_2^2 r_3^2 + r_3^2 r_1^2)}. \quad (20)$$

All eigenvalues  $r_i$ ,  $i > 3$ , are identically zero, *i. e.* even for small  $R^2$  the system is only three-dimensional independently of  $D$ . The exponent  $\alpha$  depends on  $D$  as  $\alpha = 2D - 5$ . The same formula, with  $\alpha = D - 3$ , also describes the distribution of eigenvalues of the purely bosonic model.

We can use equation (20) to explain the large  $R$  behaviour of the model, where in this case  $R^2 = r_1^2 + r_2^2 + r_3^2$  (because  $r_4^2 = 0$ ). When moving to large values of  $R^2$ , all configurations will be exponentially suppressed, except for those that keep the exponent  $r_1^2 r_2^2 + r_2^2 r_3^2 + r_3^2 r_1^2$  approximately constant. Given that  $R^2$  can only grow large if at least one of the eigenvalues does so as well, this can be achieved only if  $r_1^2 \sim R^2$ ,  $r_{2,3}^2 \sim \frac{1}{R^2}$ . As a consequence we can, in (20), approximately replace  $r_1 \rightarrow R$ ,  $r_{2,3} \rightarrow R^{-1}$  and  $\int dr_{2,3} \rightarrow R^{-1}$ . This gives us the distribution of  $R$  in the large  $R$  limit,

$$\rho(R) \sim R^{-\alpha}. \quad (21)$$

Since we have  $\frac{r_{2,3}^2}{R^2} \sim \frac{1}{R^4}$  (see figure 2), we find for the asymmetry parameter

$$\eta \sim \frac{1}{(R^2)^2}, \quad (22)$$



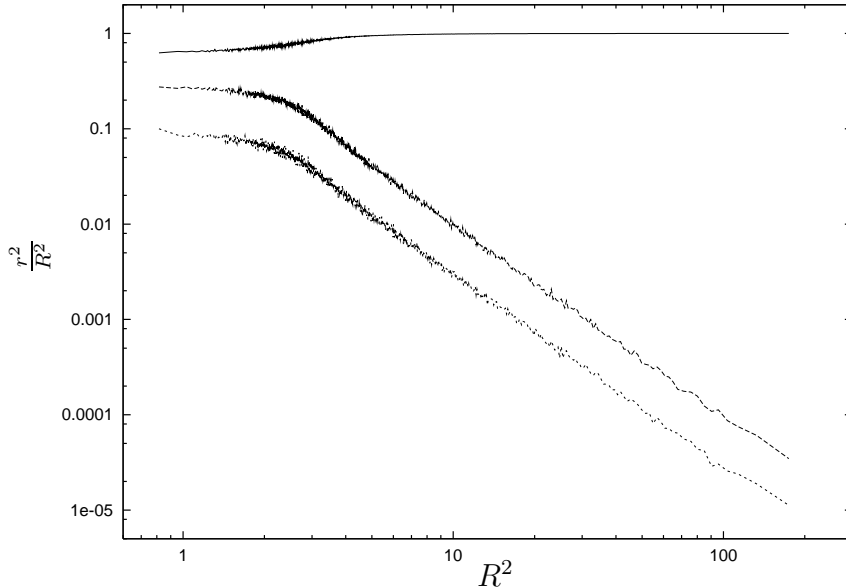


Figure 2: The eigenvalues  $r_1^2$ ,  $r_2^2$ , and  $r_3^2$ , normalized with  $R^2$ , as functions of  $R^2$  for  $N = 2$ . Note that the data has been smoothed so that each point in the figure actually represents a pair  $(\bar{R}^2, \bar{\eta})$ , with the average taken over  $n = 100$  successive values of  $R^2$ .

*i. e.*  $\eta$  goes to zero for large  $R^2$  and the quantum system becomes one-dimensional.

To summarize for  $N = 2$ : The flat directions of the bosonic part of the action, which correspond to constant values of the exponent in (20), lead to a large  $R$  behaviour of the eigenvalues  $r_1^2 \sim R^2$ ,  $r_{2,3}^2 \sim \frac{1}{R^2}$ . This is true independently of the presence or absence of fermions in the theory. However, the addition of fermions does strongly influence the power of the probability distribution  $\rho(R)$ .

Note that the flat directions being one-dimensional is a consequence of the particular form of the bosonic action; we can create systems of higher dimensions in the large  $R$  range by choosing a different action. For example, the action  $\text{Tr}[A_\mu, A_\nu][A_\nu, A_\alpha][A_\alpha, A_\mu]$  has the same symmetries as  $\text{Tr}[A_\mu, A_\nu]^2$ , but some of its flat directions are now two-dimensional. This can be seen from the eigenvalue distribution, which in this case reads

$$\rho(r) \sim (r_1 r_2 r_3)^\alpha (r_1^2 - r_2^2)(r_2^2 - r_3^2)(r_3^2 - r_1^2) e^{-24r_1^2 r_2^2 r_3^2}. \quad (23)$$

For large  $R$ , one can keep the exponent  $r_1^2 r_2^2 r_3^2$  constant by choosing  $r_1 \sim R$ ,  $r_2 \sim R$ , and  $r_3 \sim 1/R$ , which obviously describes a two-dimensional disc. In

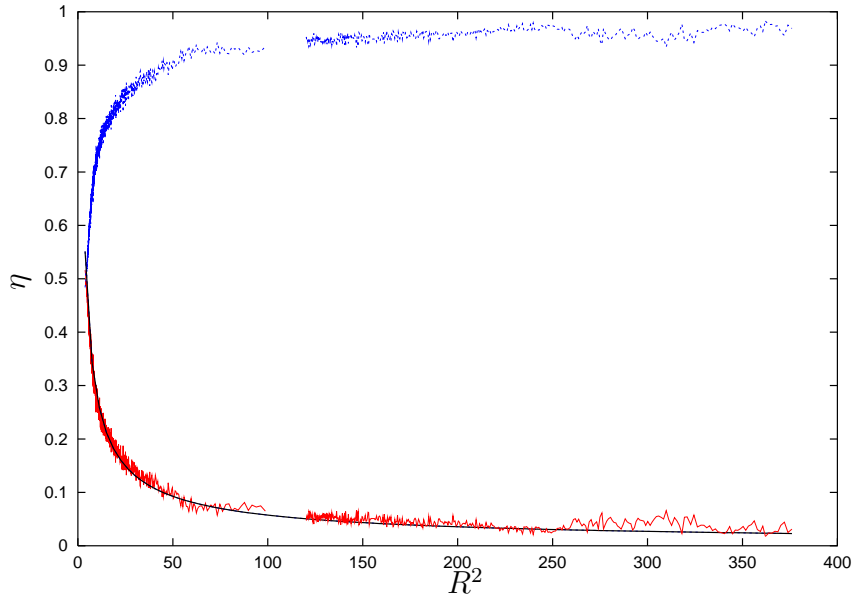


Figure 3: The plot shows  $\frac{r_1^2}{R^2}$  (upper curve) and  $\eta = \frac{r_2^2 + r_3^2 + r_3^2}{R^2}$  (lower curve) as functions of  $R^2$ , for  $N = 4$ . The data has been smoothed as explained for figure 2. The plot combines two data sets, one from an unconstrained simulation (the points for  $R^2 < 100$ ) and one from a simulation with a lower cut-off  $R_{min}^2 = 120$ . The solid line is the best power-like fit to the data from the unconstrained simulation.

this case  $\eta(R)$  goes toward a constant for large  $R$ . This type of asymmetry could be traced by a higher dimensional counter-term of  $\eta$ ,  $\eta_2 = 1 - \frac{r_1^2 + r_2^2}{R^2}$ , which would vanish for large  $R$ .

Coming back to the standard model, we can now use Monte Carlo simulations to repeat the same analysis for  $N \geq 3$ . Figure 3 shows the numerical data for  $\eta$  measured as a function of  $R^2$  for  $N = 4$ . As for  $N = 2$ , for large  $R^2$ ,  $\eta$  vanishes – in other words, the main contribution to the square extent comes from the elongated direction of what is thus an essentially one-dimensional system.

We fitted the data to a power-law function  $\eta = a(R^2)^b$ , and found for  $N = 4$  as the best fit  $a = 1.378(7)$  and  $b = -0.690(4)$ . To test the stability of this result in the region of large  $R^2$ , we repeated the simulation with the inclusion of a lower bound  $R_{min}^2 = 120$  as discussed in the previous section, to see whether the validity of the fit goes beyond the range of  $R^2$  generated in the first run. The results are collected in figure 3, and do indeed show good agreement with the results of the first simulation.

Finally, we collect the results of the best power-law fits to  $\eta$  for  $N = 3, 4, 5, 6, 8$  in the following table. For comparison, we also include the results for the surface model with  $n_T = 8, 12, 20, 28$  triangles.

$N$	$b_{matrix}$	$n_T$	$b_{surface}$
3	-0.825(2)	8	-1.604(16)
4	-0.690(4)	12	-1.463(19)
5	-0.606(4)	20	-1.412(15)
6	-0.562(5)	28	-1.383(20)
8	-0.503(29)		

In both the matrix and the surface model, the exponent  $b$  changes with  $N$ . If we assume the finite size corrections to be of order  $\frac{1}{N}$ , that is  $b(N) = b_\infty + \frac{c}{N}$ , we can try to estimate  $b_\infty$  from a fit to the measured values. For the matrix model, this leads to  $b_\infty = -0.35(1)$ ,  $c = -1.37(4)$ . We also see that  $b_\infty$  stays negative and far from zero if we assume a different kind of finite size correction, like  $\frac{1}{N^2}$  or  $\frac{1}{\sqrt{N}}$ . Thus, the data suggests that the dominance of one-dimensional configurations in the large  $R$  part of the spectrum should also be present in the limit of  $N \rightarrow \infty$ . To answer this question conclusively, however, one should extend the simulations to larger values of  $N$ .

Another related issue is the scaling of the gyration radius with  $N$ . From results of the one-loop approximation [8], one expects the maximum of the gyration radius distribution to scale as  $\sqrt{R_{max}^2}(N) \sim N^{1/4}$ , corresponding to the Hausdorff dimension  $d_H = 4$  of branched polymers which appear naturally in this approximation. Indeed, if we fit our numerical results for the surface model to the formula  $\sqrt{R_{max}^2}(N) = aN^b$ , we find  $a = 0.573(4)$  and  $b = 0.234(4)$ , which is close to  $1/4$  even though the surfaces we studied are quite small ( $n_T = 12, \dots, 60$ ). Alternatively, we can do the same using another quantity  $\hat{R}$ , which was defined in [11] as an alternative estimate of the system extent :

$$\hat{R} = \frac{1}{N} \sum_i |X_i - X_{CM}|. \quad (24)$$

Here, the best power-like fit gives  $a = 0.579(6)$  and  $b = 0.204(4)$ , which does not differ too much from the values obtained for the generic definition of the gyration radius. Presumably, for larger values of  $N$  we should see  $b$  converging to  $1/4$  for either definition.

In the matrix model, on the other hand, the situation looks quite different in the simulated range of  $N$ . Namely, in this case the best fit to  $\sqrt{R_{max}^2}(N) = aN^b$  is  $a = 1.03(4)$  and  $b = 0.81(6)$ , which means  $d_H = \frac{1}{b} = 1.23(9)$ . This is far away from the result of the one-loop approximation,  $d_H = 4$ . However,

one should note that the simulated systems are rather small for branched polymers to fully develop. Indeed, in [11] a semi-classical analogon of  $\widehat{R}$  constructed from commuting coordinates was studied for values of  $N$  in the range  $N = 16, \dots, 48$ , and its average was estimated to behave as  $\langle \widehat{R}_{sc} \rangle_N \sim N^{1/4}$ , which should also mean  $\langle \sqrt{R^2} \rangle_N \sim N^{1/4}$ .

Let us close this section with a remark about the definition of dimensionality of the system. There are two natural possibilities : the Hausdorff dimension  $d_H$ , and the effective dimension coming from the principal component analysis of the correlation matrix  $C_{\mu\nu}$ . The former describes the relation between the system size and its average extent, whereas the latter gives the minimal dimensionality of the subspace to which we can restrict our description of the system without neglecting important degrees of freedom. The two may differ in general, and it is an important physical question which definition should be used for any given problem [18].

## Conclusions

We have shown that the underlying geometry that can be associated with the field configurations of reduced supersymmetric Yang-Mills integrals in  $D = 4$  dimensions shrinks in the limit of large  $R^2 = \frac{1}{N} \text{Tr} A_\mu^2$  to an essentially one-dimensional tube. The original rotational symmetry of the action is spontaneously broken to the direction of the tube. The same mechanism has already been observed in numerical simulations of the corresponding surface model.

The origin of the power-like behaviour boils down to the existence of flat directions in the bosonic part of the action. The tubes correspond to field configurations that expand along the valleys of these flat directions, where they do not have to pay the usual ‘exponential price’, but rather one that is only power-like. The exact value of this power comes from the prefactor, which depends on the dimensionality of the problem. However, it seems that the power does not change with  $N$ . For  $D = 4$ , the distribution of the gyration radius was determined as  $\rho(R) \sim R^{-3}$ .

The analysis presented in this paper should be applicable to the six- and ten-dimensional cases as well, where one expects a distribution  $\rho(R) \sim R^{-2D+5}$ . In the large  $N$  limit we expect the estimator of the linear system extent as defined by  $R_k \equiv \langle R^{2k} \rangle^{\frac{1}{2k}}$  to pick up the singularity for  $k$  large enough, which may lead to a different scaling with  $N$  and thus a different Hausdorff dimension. A similar thing happens for example with Lévy random walks, which are known to have a Hausdorff dimension smaller than two [19]. For the IKKT model in particular, an eigenvalue distribution with a

power-like tail as the one suggested here would mean that we should expect higher-order correlators starting with  $k \geq 7$  to effectively sample the tail of the distribution, which is dominated by one-dimensional configurations.

## Acknowledgments

We thank Jan Ambjørn, Piotr Bialas, Jun Nishimura and Matthias Staudacher for discussions. The work was partially supported by the EC IHP network *HPRN-CT-1999-000161* and the KBN grant 2P03B00814.

## References

- [1] T. Eguchi and H. Kawai, *Phys. Rev. Lett.* **48** (1982) 1063.
- [2] D. J. Gross and Y. Kitazawa, *Nucl. Phys.* **B206** (1982) 440.
- [3] A. V. Smilga, *Nucl. Phys.* **B266** (1986) 45.
- [4] P. Yi, *Nucl. Phys.* **B505** (1997) 307.
- [5] S. Sethi and M. Stern, *Comm. Math. Phys.* **194** (1998) 675.
- [6] N. Ishibashi, H. Kawai, Y. Kitazawa and A. Tsuchiya, *Nucl. Phys.* **B498** (1997) 467.
- [7] W. Krauth, J. Plefka and M. Staudacher, *Class. Quant. Grav.* **17** (2000) 1171-1179.
- [8] H. Aoki, S. Iso, H. Kawai, Y. Kitazawa and A. Tada, *Prog. Theor. Phys.* **99** (1998) 713.
- [9] W. Krauth, H. Nicolai and M. Staudacher, *Phys. Lett.* **B431** (1998) 31.
- [10] W. Krauth and M. Staudacher, *Phys. Lett.* **B453** (1999) 253.
- [11] J. Ambjørn, K. N. Anagnostopoulos, W. Bietenholz, T. Hotta and J. Nishimura, *JHEP* **0007** (2000) 013.
- [12] J. Ambjørn, K. N. Anagnostopoulos, W. Bietenholz, T. Hotta and J. Nishimura, *hep-lat/0009030*.
- [13] J. Ambjørn, K. N. Anagnostopoulos, W. Bietenholz, T. Hotta and J. Nishimura, *JHEP* **0007** (2000) 011.

- [14] I. Bars, Phys. Lett. **B245** (1990) 35.
- [15] M. Fukuma, H. Kawai, Y. Kitazawa and A. Tsuchiya, Nucl. Phys. **B510** (1998) 158.
- [16] S. Oda and T. Yukawa, Prog. Theor. Phys. **102** (1999) 215.
- [17] P. Bialas, Z. Burda, B. Petersson and J. Tabaczek, Nucl. Phys. **B591** (2000) 1.
- [18] J. Nishimura and G. Vernizzi, JHEP **0004** (2000) 015.
- [19] J.-P. Bouchaud and A. Georges, Phys. Rep. **195** (1990) 127.